Highlights of Spanish Astrophysics XII, Proceedings of the XVI Scientific Meeting of the Spanish Astronomical Society held on July 15 - 19, 2024, in Granada, Spain. M. Manteiga, F. González Galindo, A. Labiano Ortega, M. Martínez González, N. Rea, M. Romero Gómez, A. Ulla Miguel, G. Yepes, C. Rodríguez López, A. Gómez García and C. Dafonte (eds.), 2025

The Missing Sulfur Problem: H_2S/OCS ratio in the warm inner core of 24 Class 0/I protostars from the Perseus Cloud

Miranzo-Pastor, J. J.[1], Fuente, A.[1], Navarro-Almaida, D.[1], Pineda, J.[2], and Segura-Cox, D.[3]

[1] Centro de Astrobiología (CAB), CSIC-INTA, Ctra.deTorrejón a Ajalvir km 4, 28806, Torrejón de Ardoz, Spain
[2] Max Planck Institute for Extraterrestrial Physics, Gießenbachstraßse 1, D-85748 Garching bei München, Germany
[3] Department of Astronomy, The University of Texas at Austin, 2515 Speedway, Austin, TX 78712, USA

Abstract

We present the preliminar results of our study of the H_2S and OCS abundances towards the warm cores associated with 24 Young Stellar Objects in the Perseus molecular cloud. This work is based in observations carried out with the NOEMA interferometer within the project PRODIGE. We calculate H_2S and OCS column densities and study variations of the H_2S/OCS ratio in our sample.

1 Introduction

Sulfur is the tenth most abundant element in the Universe, with a cosmic abundance of 10^{-5} [2]. This value has been measured in the solar system and is also compatible with the sulfur observed in the low-density interstellar medium (ISM), where all the sulfur appears to be in the gas-phase. However, the denser ISM, such as molecular clouds, and the early stages of star formation do not show the same gas-phase abundance, but around two orders of magnitude lower [3][4]. Here arises the known as the Missing Sulfur Problem, which tries to explain where the sulfur in these denser regions is hidden. One of the most accepted hypothesis claims that sulfur is locked in H_2S ices in the denser ISM, but the observation of the corresponding H_2S transitions in the ice has been extremely challenging, to the point where ice-H_2S has not been observed to the date. To loop around this problem, H_2S observations have been proposed in the inner core of protostars, where higher temperatures sublimate the ices and, with them, the H_2S gets to the gas phase. On the other hand, H_2S ices photodissociation leads to the formation of OCS ices [5], which will be in the gas phase as well as the H_2S in the warm core of protostars. Our final goal is to study and understand how the H_2S/OCS ratio varies in a set of 24 Class 0/I protostars from the Perseus Cloud. Here, we present the first results of our work, still in progress to this date.

2 Observations

This work is based on observations of the MPG-IRAM Observing Program PRODIGE (Project ID: L19MB; PIs: Paola Caselli, Thomas Henning). Within this program, a series of 24 Class 0/I protostars have been observed with the NOrthern Extended Millimeter Array (NOEMA). In this program, the Band 3 receiver and the PolyFix correlator were used. PolyFix provides ∼15.5 GHz of bandwidth (divided into two 7.744 GHz wide sidebands separated by 15.488GHz). The whole band was observedd with a spectral resolution of 2 MHz. Moreover, several windows with high spectral resolution, 62.5 kHz channel width, were located to observe some interesting lines.

We processed the NOEMA observations from uncalibrated data using the standard observatory pipeline in the Grenoble Image and Line Data Analysis Software (GILDAS) package Continuum and Line Interferometer Interferometer Calibration (CLIC). We used 3C84 and 3C454.3 as bandpass calibrators. 0333+321 and 0333+322 were used for phase and amplitude calibration, with observations for these calibrators taken every 20 min. Flux calibration sources were LKHA101 and MWC349. The uncertainty in flux density was 10%. The continuum was bright enough to allow for self-calibration.

Table 1: List of studied NOEMA lines in order of increasing wavelength.

ν (GHz)	Species	Transition Upper - Lower	A_{ij} $\log(s^{-1})$	E_u (K)	Δv (kHz)	RMS (mJy/beam)
215.5029	$H_2^{33}S$	2(2,0)4−2(1,1)4	-3.772	81.6	2000	[2.0-2.9]
216.7104	H_2S	2(2,0)−2(1,1)	-4.312	84.0	2000	[2.0-2.9]
216.1474	$OC^{33}S$	J = 18 − 17	-4.420	98.6	62.5	[15-60]
218.9034	OCS	J = 18 − 17	-4.517	99.8	62.5	[10-50]
231.0615	OCS	J = 19 − 18	-4.446	111	62.5	[20-80]
237.2736	$OC^{34}S$	J = 20 − 19	-4.411	120	2000	[2.5-3.5]

Notes: Δv is the spectral resolution with which the transition was observed. In RMS we give a range for the typical noise in the datacubes of each transition.

3 Results

In this section, we explain how we have obtained the moment-0 maps and the spectra of the warm inner core of the 24 protostars of our sample. We then show how we have derived the column densities and abundances of the different species. As an example, we display the different features of Class 0/I protostar SVS13A.

3.1 Moment-0 maps

In Fig. 1 we present as a example the moment-0 maps of SVS13A, showing the emission of the H_2S, OCS(18-17) and OCS(19-18) lines. We created the moment-0 maps by integrating the data cubes over specific velocity ranges for each map. Integration of the maps was done over a threshold of 3σ, specific for each cube. Typical noise values for each line are given in Table 1.

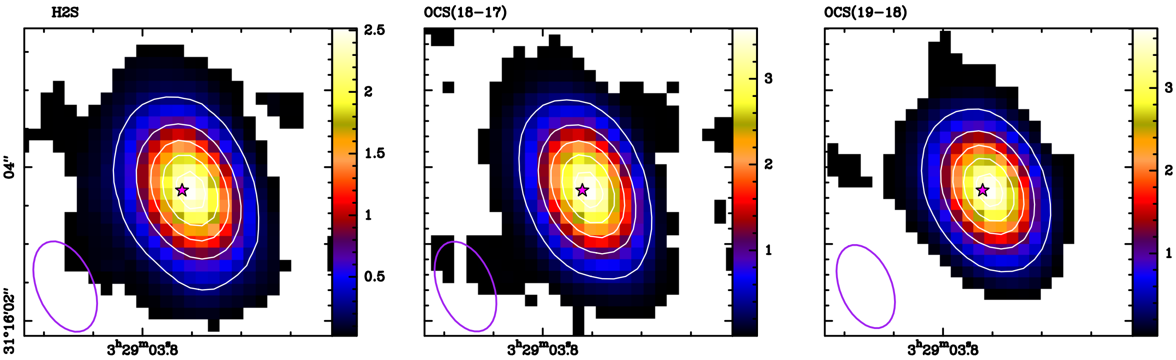

Figure 1: Moment-0 maps of the H_2S and OCS lines in SVS13A. The color map displays the emission ($>3\sigma$) of the species. The colorbar indicates the intensity of the emission, in K km s^{-1}. White contour lines show 10-30-50-70-90% of the peak emission. To complement this representation, we also plotted the size of the beam, represented by a purple ellipse in the bottom-left corner. The position of the peak of the continuum is marked with a pink star.

In the maps, we see that the H_2S line usually appears centered in the peak of the continuum, while the OCS can be sometimes detected in slightly displaced regions, and with more asymmetric spatial distributions. We also find that OCS is only observed in sources where H_2S was detected, and that OCS(18-17) and OCS(19-18) are always detected together. Regarding the isotopologues, we find that many of the OCS detections are also detected in $OC^{34}S$. This is a clear indicator of optically thick OCS lines. We have assumed an isotopic ratio, $^{32}S/^{34}S$, of 22.5 [6]. The isotopologue ^{33}S is even scarcer than its 34 isotope counterpart, but the value of the $^{34}S/^{33}S$ ratio has not been uniformly established, as it may change depending on the region. The standard value is 6.27 ± 1.01 [6][7].

3.2 Spectra

To obtain the emission of the different molecules in the warm inner core, we needed to integrate the spectra of only the most interior region of the protostar. We decided to extract the spectra of a circular region of 1.5"×1.5" around the peak of the continuum for every source. After extracting all the spectra, we fitted a Gaussian profile to the detected lines

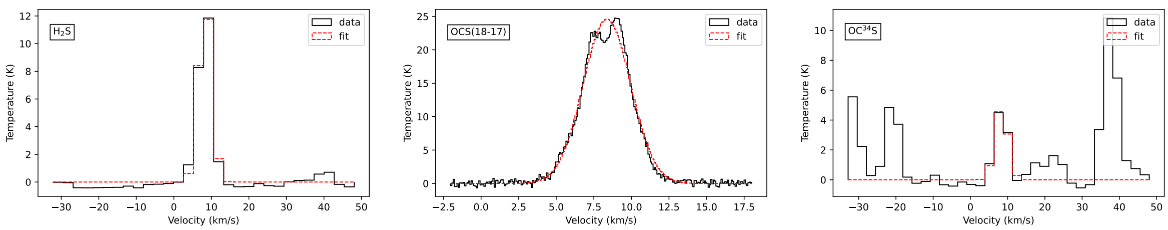

Figure 2: Integrated spectra of the $H_2S(2(2,0)-2(1,1))$, OCS(18-17) and $OC^{34}S$(20-19) lines in the warm inner core of SVS13A. The black histogram shows the emission of each species. The red profile is the Gaussian fit to the emission line.

using the `CLASS` software from `GILDAS`.

In Fig 2, we present the integrated spectra of the H_2S 2(2,0)–2(1,1), the OCS (18–17) and the $OC^{34}S$ (20–19) lines in the warm inner core (1.5” ×1.5”) of SVS13A. Considering the whole sample, we find clear detections ($>5\sigma$) of both H_2S and OCS in most of the sources while $OC^{34}S$ detections are usually more faint ($>3\sigma$) or temptative ($<3\sigma$). We also extracted the spectra of the OCS (19–18), the $OC^{33}S$ (20–19) and the $H_2^{33}S$ 2(2,0)–2(1,1) lines.

3.3 Column densities and abundances

We calculated column densities for OCS, as well as for H_2S. In the cases where H_2S was detected but OCS emission was not detected, we estimated an upper limit to the column density of OCS. Total column densities have been calculated assuming local thermodynamic equilibrium (LTE) and a $T_{\rm ex}$ of 100K, or $T_{\rm ex} = T_{\rm bol}$ if $T_{\rm bol} > 100K$, in the warm inner core, for all species and sources. We estimated an additional value for the column densities of OCS and H_2S, when possible, using their isotopologues $OC^{34}S$ and $H_2^{33}S$. The column densities of H_2S and $H_2^{33}S$ have been calculated assuming an *orto*/*para* ratio of 3.

4 H_2S/OCS ratio

We have calculated the averaged column densities of H_2S, $H_2^{33}S$, OCS, $OC^{34}S$, and $OC^{33}S$ in a 1.5” diameter circle around the continuum peak using the averaged interferometric spectra and following the procedure described in the previous section.

One important problem we have faced is the impact that the opacity of the main species’ lines can have in our column density estimates, leading to a severe underestimation of the real values. To avoid this problem, we use the observations of the less abundant isotopologues as a proxy of the most abundant one. We have detected the $OC^{34}S$ line in ∼75% of the targets detected in OCS. Significant deviations of the ^{32}S/ ^{34}S ratios from the solar value are not detected in the interstellar medium and/or comets [8]. Therefore, we use $OC^{34}S$ as a proxy for OCS by calculating $N(\rm OCS)=22.5\times N(OC^{34}S)$. We have also detected the $OC^{33}S$ line in 9 protostars. The values of $N(OC^{34}S)/N(OC^{33}S)$ in these targets are > 2.5, proving that the $OC^{34}S$ line is not optically thick.

Table 2: Column densities and H_2S/OCS ratios in Perseus.

Protostar	Class	$T_{\rm bol}$ (K)	$T_{\rm kin}$ (K)	N(OCS) (cm^{-2})	N(H_2S) (cm^{-2})	H_2S / OCS
B1bN	0	14.7	100.0	0.0	$(1.54\pm1.31)\times10^{15}$ $^{(b)}$	-
B1bS	0	17.7	100.0	$(2.88\pm1.12)\times10^{15}$ $^{(a)}$	$(2.65\pm0.08)\times10^{16}$ $^{(b)}$	$9.21^{+4.33}_{-2.79}$
B5-IRS1	I	287.0	287.0	$<7.15\times10^{13}$	$(5.04\pm1.26)\times10^{14}$	>7.04
HH211	0	27.0	100.0	$(1.60\pm0.87)\times10^{15}$ $^{(a)}$	$(2.10\pm0.17)\times10^{14}$	$0.132^{+0.125}_{-0.053}$
IC348MMS	0	30.0	100.0	$(1.97\pm0.30)\times10^{15}$ $^{(a)}$	$(2.94\pm0.01)\times10^{16}$ $^{(b)}$	$14.9^{+1.9}_{-2.0}$
IRAS2A	0/I	69.0	100.0	$(1.85\pm1.16)\times10^{16}$ $^{(a)}$	$>5.69\times10^{16}$ $^{(b)}$	>3.08
IRAS2B	I	106.0	106.0	$(1.06\pm0.21)\times10^{14}$	$(1.03\pm0.15)\times10^{14}$	$0.973^{+0.333}_{-0.283}$
IRAS4B	0	28.0	100.0	$(1.44\pm0.39)\times10^{16}$ $^{(a)}$	$(2.06\pm0.01)\times10^{17}$ $^{(b)}$	$14.3^{+3.6}_{-3.1}$
IRAS4C	0	31.0	100.0	$(3.89\pm1.38)\times10^{13}$	$(1.15\pm0.13)\times10^{14}$	$2.97^{+1.53}_{-1.02}$
L1448-IRS3A	I	47.0	100.0	$(2.17\pm1.16)\times10^{15}$ $^{(a)}$	$(2.18\pm0.46)\times10^{14}$	$0.101^{+0.115}_{-0.049}$
L1448-IRS3B	0	57.0	100.0	$(1.61\pm0.76)\times10^{15}$ $^{(a)}$	$(2.71\pm0.12)\times10^{14}$	$0.168^{+0.112}_{-0.059}$
L1448C	0	47.0	100.0	$(3.82\pm3.69)\times10^{15}$ $^{(a)}$	$(1.31\pm0.03)\times10^{15}$	$0.34^{+6.44}_{-0.17}$
L1448NW	0	22.0	100.0	$<3.43\times10^{13}$	$(9.61\pm2.63)\times10^{13}$	>2.81
Per-emb-2	0	27.0	100.0	$(2.79\pm1.11)\times10^{13}$	$(3.00\pm0.15)\times10^{14}$	$10.8^{+5.5}_{-3.4}$
Per-emb-5	0	32.0	100.0	$(1.91\pm0.58)\times10^{15}$ $^{(a)}$	$(1.48\pm0.11)\times10^{14}$	$0.078^{+0.030}_{-0.022}$
Per-emb-8	0	43.0	100.0	$<2.92\times10^{13}$	$(1.16\pm0.30)\times10^{14}$	>3.98
Per-emb-18	0	59.0	100.0	$(3.65\pm0.55)\times10^{15}$ $^{(a)}$	$(2.77\pm0.13)\times10^{14}$	$0.076^{+0.013}_{-0.013}$
Per-emb-22	0	43.0	100.0	$(2.37\pm0.15)\times10^{14}$	$(3.79\pm0.13)\times10^{14}$	$1.60^{+0.13}_{-0.15}$
Per-emb-29	0	48.0	100.0	$(4.51\pm2.03)\times10^{15}$ $^{(a)}$	$(5.36\pm0.09)\times10^{16}$ $^{(b)}$	$11.9^{+6.8}_{-3.8}$
Per-emb-30	0/I	78.0	100.0	0.0	0.0	-
Per-emb-50	I	128.0	128.0	0.0	0.0	-
Per-emb-62	I	378.0	378.0	0.0	0.0	-
SVS13A	0/I	188.0	188.0	$(4.33\pm2.70)\times10^{16}$ $^{(a)}$	$>1.48\times10^{17}$ $^{(b)}$	>3.42
SVS13B	0	20.0	100.0	$(1.39\pm0.64)\times10^{15}$ $^{(a)}$	$(2.68\pm0.19)\times10^{14}$	$0.19^{+0.13}_{-0.07}$

Notes: $^{(a)}$ Estimated using the $OC^{34}S$ isotopologue column density. $^{(b)}$ Estimated using the $H_2^{33}S$ isotopologue column density.

In the case of H_2S, we have detected the $H_2^{33}S$ 2(2,0)-2(1,1) in six sources. In these sources, we used the $H_2^{33}S$ column density to compute that of H_2S assuming $^{32}S/^{33}S = 125$. The column densities thus calculated are significantly higher than those estimated from the main isotopologue line. The most extreme case is B1bS, in which the column density estimated from $H_2^{33}S$ is $\sim$ 144 higher than that obtained from the main isotopologue observations. However, the difference is lower, $\sim$ 13 to $\sim$ 84, for the other protostars.

The values of H_2S/OCS range from $\sim$0.1 to $\sim$15, thus expanding over 2 orders of magnitude, as we show in Table 2. In fact, we can differentiate two groups. The first one, characterized by H_2S/OCS $\sim$ 10-15, is formed by 4 of the sources detected in $H_2^{33}S$ and one additional source with low OCS column density and we will refer to them as "OCS-poor" targets. The second one is composed of 9 sources with N(H_2S) $< 2\times10^{15}$ cm^{-2} and presents H_2S/OCS $\sim$ 0.1-3. We will refer to these targets as "OCS-rich" protostars. In 3 sources, we have not detected OCS and only upper limits to the H_2S/OCS ratio can be derived. These limits imply H_2S/OCS >3 and we will consider them as "OCS-poor" protostars. We consider that this differentiated chemistry can be related with a different composition of the sublimated ice.

5 Summary and Conclusions

In this work, we studied several sulfur-bearing species —H_2S, $H_2^{33}S$, OCS, $OC^{33}S$, $OC^{34}S$— in the warm inner core of 24 Class 0/I protostars in the Perseus Cloud. We calculate average gas-phase column densities of H_2S, $H_2^{33}S$, OCS, $OC^{33}S$ and $OC^{34}S$ in a 1.5"-diameter circle ($\sim$500 au at the distance of Perseus) around the protostar. We detected H_2S in 21 of the 24 sources in our sample, and OCS in 17 of them. We found that protostars can be characterized by their H_2S and OCS composition. We differentiate two kinds of objects: OCS-poor protostars, with H_2S/OCS$\sim$9-15; OCS-rich protostars, with H_2S/OCS$\sim$0.1-3. We interpret that these differences in the H_2S/OCS ratio are more likely reflecting a different composition in the pre-stellar phase and/or a different dynamical history.

Acknowledgments

This work is supported by ERC grant SUL4LIFE, GA No. 101096293. Funded by the European Union. Views and opinions expressed are however those of the author(s) only and do not necessarily reflect those of the European Union or the European Research Council Executive Agency. Neither the European Union nor the granting authority can be held responsible for them.

References

[1] Artur de la Villarmois, E., et al, 2023, A&A, 678, A124

[2] Asplund, M., 2009, ARA&A, 47, 481

[3] Vastel, C., et al. 2018, MNRAS, 478, 5514

[4] Rodríguez-Baras, et al, 2021, A&A, 648, A120

[5] el Akel, M., et al, 2022, A&A, 659, A100

[6] Anders, E. and Grevesse, N., 1989, Geochim. Cosmochim. Acta, 53, 197

[7] Chin, Y. N., et al, 1996, A&A, 305, 960

[8] Calmonte, U., et al, 2017, MNRAS, 469, S787